Modelling of a proton spot scanning system using MCNP6

2017 J. Phys.: Conf. Ser. 860 012025

(http://iopscience.iop.org/1742-6596/860/1/012025)

IOP Conf. Series: Journal of Physics: Conf. Series **860** (2017) 012025 doi:10.1088/1742-6596/860/1/012025

Modelling of a proton spot scanning system using MCNP6

O Ardenfors[1,5], A Dasu[2,3], M Kopeć[4] and I Gudowska[1]

[1] Medical Radiation Physics, Department of Physics, Stockholm University, Stockholm, Sweden
[2] The Skandion Clinic, Uppsala, Sweden
[3] Department of Medical and Health Sciences, Linköping University, Linköping, Sweden
[4] Department of Nuclear Energy, Faculty of Energy and Fuels, University of Science and Technology, Krakow, Poland

[5] Corresponding author e-mail: oscar.ardenfors@fysik.su.se

Abstract. The aim of this work was to model the characteristics of a clinical proton spot scanning beam using Monte Carlo simulations with the code MCNP6. The proton beam was defined using parameters obtained from beam commissioning at the Skandion Clinic, Uppsala, Sweden. Simulations were evaluated against measurements for proton energies between 60 and 226 MeV with regard to range in water, lateral spot sizes in air and absorbed dose depth profiles in water. The model was also used to evaluate the experimental impact of lateral signal losses in an ionization chamber through simulations using different detector radii. Simulated and measured distal ranges agreed within 0.1 mm for R_{90} and R_{80}, and within 0.2 mm for R_{50}. The average absolute difference of all spot sizes was 0.1 mm. The average agreement of absorbed dose integrals and Bragg-peak heights was 0.9%. Lateral signal losses increased with incident proton energy with a maximum signal loss of 7% for 226 MeV protons. The good agreement between simulations and measurements supports the assumptions and parameters employed in the presented Monte Carlo model. The characteristics of the proton spot scanning beam were accurately reproduced and the model will prove useful in future studies on secondary neutrons.

1. Introduction

The interaction properties of protons enabling substantial energy depositions in the Bragg peak at well-defined depths have established proton radiation therapy as a suitable option for treating tumors with considerable sparing of the surrounding normal tissues [1-3]. In recent years there has been an increase in the use of spot scanning technique for the delivery of proton therapy using magnets to laterally scan the target by one narrow proton beam at a time and using different nominal energies to adjust the range of protons to deliver the required dose to the whole target volume.

The properties of proton beams can vary substantially between different proton facilities and should be characterized to allow for an independent validation of the performance of the treatment planning system (TPS). In order to characterize a proton beam a verification of different physical quantities such as depth and lateral dose distribution is essential. This verification can be performed by modelling the proton interactions, the beam transport through the beamline and the patient using Monte Carlo (MC) simulations

as this is generally the most accurate tool for such studies [3, 4]. To accurately model a proton beam, the characteristics of the beam must be established through benchmarking between MC simulations and corresponding measurements performed at the proton facility. As the primary protons undergo scattering and nuclear interactions within the patient, scattered and secondary particles can give rise to a low dose envelope surrounding the primary proton beam causing a broadening of the beam spatial distribution (commonly denoted 'halo' contribution). The effect of this low-dose envelope can lead to an increase in total dose deposition when irradiating large tumor volumes [5, 6] and its influence on the results should hence be accounted for when comparing simulations or measurements with dose distributions calculated by the TPS.

The low production of secondary particles in the treatment nozzle of spot scanning beams generally allows for excluding full treatment head simulation when modelling the beam characteristics for in-field assessment [7, 8]. Secondary particles are instead predominantly produced within the patient [9-11] and much concern exists with respect to the neutron contribution. The transport of these particles is most accurately modeled using a benchmarked MC code in which evaluated nuclear data tables and nuclear models are employed. The latest version of the Monte Carlo N-Particle transport code (MCNP6) developed at the Los Alamos National Laboratory, USA, implements evaluated nuclear data files from thermal energies up to 150 MeV and additional libraries and physics models for higher energies to simulate neutron transport [12]. This makes it a highly suitable MC code for simulation of neutrons and other secondary particles in the energy range of proton therapy [2, 13-15]. The implementation of MCNP for proton dose calculations has been previously validated against other MC codes such as GEANT4 and FLUKA [14, 16-18].

Simulations of secondary neutrons require an accurate beam transport model with proper beam characteristics benchmarked with experimental measurements. The aim of this work was to create a MC model using the code MCNP6 (ver. MCNP6.1.1 released in 2014) based on input parameters obtained from measurements performed at beam commissioning. The model was used to benchmark simulations of absorbed doses against measurements to allow for future studies of the production of secondary neutrons doses using the advantages of MCNP6. The MC model was also used to simulate the influence of lateral spread and beam halo with regard to signal losses when performing measurements using a commercially available plane parallel ionization chamber (IC).

2. Material and Methods

2.1. Measured data

All measurements were performed on a dedicated spot scanning proton facility with a maximum cyclotron energy of 230 MeV from IBA (Ion Beam Applications, Louvain-La-Neuve, Belgium) recently installed at the Skandion Clinic, Uppsala, Sweden. Integral depth dose (IDD) curves in water for nominal proton energies between 60 and 226 MeV in steps of 5 MeV were obtained from measurements performed at commissioning using a PTW 34070 Bragg peak plane-parallel IC with an active radius of 4.08 cm (PTW-Freiburg, Freiburg, Germany). The IC was irradiated in water with a single spot beam with a fixed energy at a time. The output air ionization signal from the IC was converted to that corresponding to dose to water using stopping power ratio values calculated using equation B.13 in TRS-398 [19]. This conversion corresponds to an uncertainty of 1% in a clinical proton beam [19].

Beam profile measurements in air were carried out in energy intervals of 10 MeV from 60 to 226 MeV using a Lynx scintillation detector with a pixel resolution of 0.5 mm x 0.5 mm (IBA dosimetry, Schwarzenbruck, Germany). The detector was irradiated at five positions along the beam axis for each energy: -19 cm, -10 cm, 0 cm, +10 cm and +20 cm (positions relative to isocenter). The nozzle exit was located at approximately -53 cm relative to isocenter. Standard deviations of the beam Gaussian spatial

distribution (denoted spot sizes henceforth) in the x- and y-direction ($\sigma_{x,y}$) were obtained from the measured beam profiles in air for all positions and energies.

Absorbed dose assessment was carried out for nominal energies from 60 to 226 MeV in 5 MeV intervals through measurements using two ionization chambers calibrated in terms of absorbed dose to water at the National Metrology Laboratory for ionising radiation. A cylindrical FC65-G chamber (IBA dosimetry, Schwarzenbruck, Germany) was used for nominal energies above 150 MeV and a plane-parallel Roos electron chamber (PTW-Freiburg, Freiburg, Germany) was used for lower energies. The chamber was irradiated with a homogeneous 10 cm x 10 cm field using a spot separation of 2.5 mm. The absorbed dose at reference depth, D_{cal}, was determined and equation (1) was used to calculate a standardization factor at the reference depth, D_{ref}, in units of Gy·mm^2/MU relating the number of monitor units (MU) to the dose determined at the reference depth. The reference depth in water was 3 cm for beams with nominal energies above 150 MeV. For lower energies the reference depth was at 2 cm to prevent the chamber being placed at the proximal rise of the depth dose curve.

$$D_{ref} = D_{cal} \times \frac{SAD_{factor}}{MU_{factor}} \tag{1}$$

where MU_{factor} is the number of MU delivered per proton spot multiplied with the number of spots per mm^2. The source-axis distance factor (SAD_{factor}) corrects for the distance between reference depth, d_{ref}, and position of the MU reference chamber in the treatment nozzle, d_{MU}. The SAD_{factor} is calculated with equation (2), where SAD_x=1830 mm and SAD_y=2203 mm are the distances from isocenter to the virtual source position on the two axes.

$$SAD_{factor} = \frac{\left(SAD_x - d_{ref}\right) \times \left(SAD_y - d_{ref}\right)}{\left(SAD_x - d_{MU}\right) \times \left(SAD_y - d_{MU}\right)} \tag{2}$$

The standardization factor at reference depth, D_{ref}, was then used to convert the IDD curves measured for single spot irradiations under non-reference conditions, IDD_{spot}, into units of Gy·mm^2/MU using equation (3).

$$IDD_{abs} = IDD_{spot} \times \frac{D_{ref}}{IDD_{spot}^{ref-depth}} \tag{3}$$

where $IDD_{spot}^{ref-depth}$ is the value on the IDD curve for the spot irradiation at the reference depth (2 or 3 cm depending on energy) and IDD_{abs} is the measured IDD curve converted into units of Gy·mm^2/MU.

2.2. Modelling of integral depth dose and lateral beam size

Proton beams of energies from 60 MeV to 226 MeV in steps of 5 MeV were individually simulated and modelled. The ionization energy losses of the protons in water were evaluated in MCNP6 using the Bethe-Bloch formula with a mean excitation potential of 75.3 eV. The number of multiple scattering points was set to maximum by decreasing the energy spacing to minimum with the MCNP parameter efac set to 0.99 [20]. The nuclear interactions were simulated using the Bertini intranuclear cascade model [21]. The proton source was defined using the -41 entry on the source definition card (SDEF) corresponding to a built-in Gaussian spatial distribution. The standard deviations of the Gaussian distributions were defined using the energy specific $\sigma_{x,y}$-values obtained from the spot size measurements at -19 cm using the Lynx detector.

The beam divergence was characterized by x- and y-components which can vary depending on the different properties of the beamline such as the placement of the steering dipole magnets. For the beamline employed in this work the x-component of the spot sizes was constantly increasing with distance (divergent) for all energies whereas the y-component slightly converges before isocenter and then diverges for energies above 170 MeV. The beam divergence was simulated using an energy dependent distribution with three components: x divergence, y divergence and no divergence. For nominal energies above 170 MeV the x- and y-divergence was simulated as a cone in which the cosine angle was calculated from the difference in spot size between the -19 cm and +20 cm Lynx measurements. For lower nominal proton energies the y-divergence was set to zero. The largest divergence angle was 2.3 degrees for the x-component at 60 MeV.

The energy distribution of the primary proton beam was assumed to be normally distributed around a nominal energy with an energy-specific standard deviation, σ_E. The final value of σ_E for each initial proton energy was obtained through an iterative process in which the nominal proton energy was held constant and σ_E was varied. The IDD curves of each specific proton energy were then evaluated with regard to the spread of the Bragg peak and the height of the plateau. When further changes in σ_E did not improve the results the process was completed. The standard deviation of the energy distribution decreased with increasing energy from 0.8% (60 MeV) to 0.3% (226 MeV). As illustrated in Figure 1, a low energy tail was added to the Gaussian shaped energy distribution to account for the change in proton energy distribution due to primary protons scattered in the treatment nozzle. The magnitude of the low energy tail in the probability distribution function (PDF) was determined individually for each primary proton energy through repeated simulations and evaluations of the IDD curves at shallow depths. The value varied between 1.0×10^{-4} and 1.4×10^{-4} depending on the primary proton energy. The choice to use a constant value for the low energy tail was based on the assumption that the fluence of secondary protons originating from the treatment head exit is rather constant with regard to energy as shown by Grassberger et al. [8].

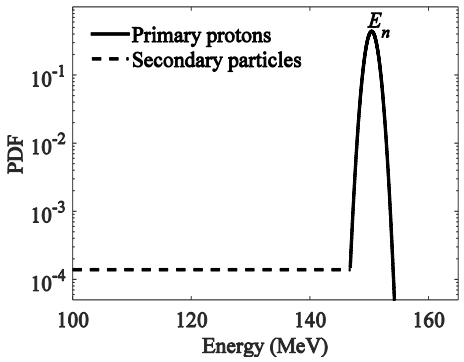

Figure 1. Probability distribution function (PDF) of proton energy distribution with nominal energy (E_n) of 150.4 MeV and energy standard deviation (σ_E) of 0.6%.

The IDD simulations were performed by scoring energy depositions in 0.1 mm thick water cylinders with radius of 4.08 cm for primary proton energies from 60 to 226 MeV in steps of 5 MeV. The simulated IDD curves were evaluated against the measured IDD curves with regard to the distal ranges R_{90}, R_{80} and R_{50}. The statistical uncertainties of all cylinder tallies were less than 0.005 for all simulated energies.

The beam profile simulations in air were simulated using an energy deposition mesh tally scoring the deposited proton energy. The mesh grid was placed at -19 cm, -10 cm, 0 cm, +10 cm and +20 cm (distances relative to isocenter) and the proton source was placed at -19 cm. Mesh sizes were defined as equal to the pixel resolution of the Lynx detector (0.5 mm x 0.5 mm). All spot sizes were calculated and compared with the corresponding spot sizes determined from the beam profiles measured with the Lynx detector.

2.3. Absorbed dose benchmarking simulations

Absorbed dose simulations were carried out using the same setup as for the reference dosimetry measurements. Thus, a water phantom was irradiated with a 10 cm x 10 cm field of 1681 proton spots with a spot separation of 2.5 mm and each proton source was defined according to the IDD simulations. The F6 tally output from MCNP6 (in MeV per unit mass per initial proton) at reference depth in the water phantom, $IDD_{MCNP}^{ref-depth}$, was calculated and used to convert the IDD curves from the single spot simulations into units of Gy·mm^2/MU with equation (4).

$$IDD_{abs}^{MCNP} = IDD_{spot}^{MCNP} \times \frac{D_{ref}}{IDD_{MCNP}^{ref-depth}} \quad (4)$$

where IDD_{abs}^{MCNP} is the simulated IDD curve in units of Gy·mm^2/MU, D_{ref} is the standardization factor calculated from measured data and IDD_{spot}^{MCNP} is the IDD curve simulated for single spots under non-reference conditions. The statistical uncertainty of $IDD_{MCNP}^{ref-depth}$ was less than 0.005 for all simulated energies.

The calculated IDD curves normalized to MU were evaluated against IDD curves derived from measurements with regard to the absolute height of the Bragg Peaks and the total dose deposition defined as the integral of the absorbed dose curves.

2.4. Lateral signal loss simulations

Signal losses due to lateral spread when performing measurements with the 4.08 cm radius PTW ionization chamber were investigated through simulations of IDD curves using an increased detector radius of 25 cm. Simulations using larger radii ensured that a radius of 25 cm was sufficient to account for all signal contribution from laterally scattered protons. The ratios between the IDD curves from the small radius (4.08 cm) simulations and the full signal simulations (25 cm radius) were calculated to evaluate signal losses at different depths for proton energies between 60 and 226 MeV in steps of 5 MeV.

3. Results

3.1. Integral depth dose in water and lateral beam size in air

Ranges derived from simulated and measured IDD agreed within 0.1 mm for R_{90} and R_{80}, and within 0.2 mm for R_{50}. Calculated differences between simulated and measured R_{90}, R_{80}, and R_{50} for all energies are presented in Figure 2a. Measured spot sizes of the x-component in isocenter ranged between 7.2 mm (60 MeV) and 2.9 mm (226 MeV), corresponding values of the y-component were 7.2 mm and 2.8 mm. The largest spot size was measured for 60 MeV at +19 cm corresponding to 8.1 mm and 7.6 mm for the x- and y-component respectively. The difference in spot size between simulations and measurements for both the x- and y-component was relatively constant for the five positions along the beam axis with the largest average difference found at +20 cm. The average difference in spot size for the five positions was 0.1 mm for both the x- and the y-component. The largest difference of the x-component was -0.6 mm for 60 MeV

at +20 cm and the corresponding value for the y-component was -0.7 mm for 65 MeV at -19 cm. The simulated spot sizes were based on the measurements at -19 cm and the reason for the difference between measurements and simulations at this position was due to the beam divergence. The percentage difference in spot sizes (simulated-measured) of the x-component are presented in Figure 2b where it is seen that all spot sizes agree within 10% (similar results for the y-component).

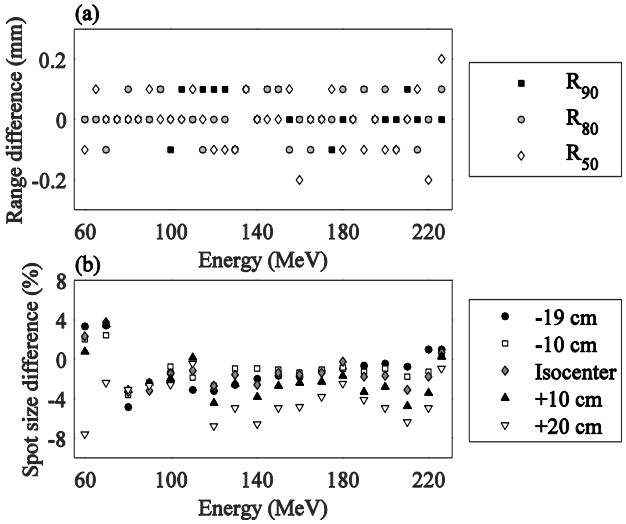

Figure 2. (a) Calculated differences in range between normalized IDD curves from simulations and measurements for proton energies in the range 60-226 MeV. (b) Percentage differences between the x-component of the spot sizes from simulations and measurements.

3.2. Absorbed dose benchmarking simulations

Absolute IDD curves in units of Gy·mm^2/MU derived from measurements and simulations using the standardization factors, D_{ref}, for energies between 60 and 226 MeV are presented in Figure 3. The average absolute difference of the IDD curve integrals derived from simulations and measurements for all energies was 0.8% and the maximum difference was 2%. The largest difference in the height of the Bragg-peak was found at 145 MeV corresponding to 2.1% (1.8 Gy·mm^2/MU) and the average absolute difference of all energies was 0.9%.

3.3. Lateral signal loss simulations

Ratios between MCNP6 simulations using a tally radius of 4.08 cm and 25 cm are presented in Figure 4 for a selection of representative energies. The signal loss of the 4.08 cm radius PTW IC increased with incident proton energy. The maximum signal loss was approximately 0.2%, 1.5%, 3.4% and 6.7% for the incident proton energies 120, 160, 190 and 226 MeV, respectively.

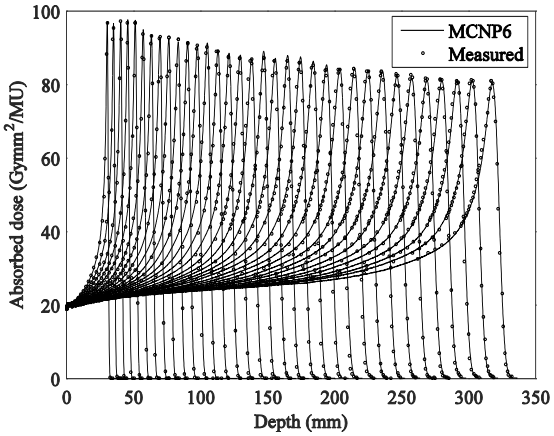

Figure 3. Absolute IDD curves for nominal beam energies in the range 60–226 MeV derived from measurements and MCNP6 simulations in water using the absorbed dose values obtained from reference measurements performed with calibrated ionization chambers.

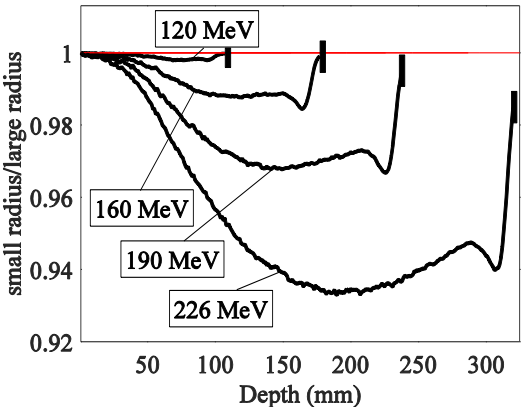

Figure 4. Calculated ratios between simulations using 4.08 cm radius and 25 cm radius for a selection of energies. The vertical markers correspond to the Bragg peak of the corresponding energy.

4. Discussion and Conclusions

In this work, the latest version of MCNP (MCNP6.1.1) has been used to model the characteristics of a dedicated proton spot scanning facility. All modelling parameters were based solely on measurements performed during commissioning and recognized assumptions regarding the energy distribution of the proton beam. The MCNP6 model has been benchmarked against measurements with regard to absorbed dose IDD normalized to the number of MU employed.

The energy distribution of the initial proton beam was defined using energy specific PDF defined with energy factors modifying the nominal primary proton energy and a Gaussian distribution defined with energy specific standard deviations. The low energy tail in the PDF of the energy distribution modelling the contribution from secondary particles scattered in the treatment head nozzle (mainly protons) resulted

in an increase in MCNP6 output at shallow depths of roughly 0.5% for lower proton energies and about 2.5% for higher energies. Thus, simulations performed without including the low energy tail in the PDF caused an underestimation of the normalized IDD curves at shallow depths in comparison to measured IDD profiles (especially for higher energies). This result does not necessarily mean that the PDF employed in this work is a full representation of the actual energy distribution of the protons exiting the treatment head but that it is a rather valid simplification supported by previous findings [8]. It should be noted that the exclusion of geometrical modelling of the treatment nozzle itself could lead to underestimations of doses to regions outside the primary proton field [8]. However, considering that most scattered radiation in treatment-like situations originates from within the patient when irradiated with a spot scanning beam [9-11] the low energy tail employed in this work is a reasonable simplification for modelling of the secondary particle contribution originating from the treatment nozzle. The agreement between the integrals of the measured and simulated IDD curves in Figure 3 supports this assumption.

The spatial distribution of the beam was simulated using standard deviations and beam divergence derived from measurements. The average differences in spot size all correspond to a full width at half maximum of less than that of the resolution of the Lynx detector (0.5 mm). The largest average difference in spot sizes between simulations and measurements was found at +20 cm relative to isocenter. Considering that the patient, or phantom, is usually positioned so that the surface is located before the isocenter this discrepancy will most likely have very little impact on spot sizes inside a medium.

The results from the simulations of IDD curves using different IC radii presented in Figure 4 confirmed previously reported results that a limited detector width can lead to an underestimation in detected energy deposition of several percent for higher energies [22-24]. The largest effect of the limited detector width was seen in the distal half of the particle track and is a result of protons undergoing elastic scattering on hydrogen and nonelastic scattering on oxygen resulting in large scattering angles [25]. The trajectories of the scattered protons naturally cause an increase in signal loss with depth as they travel away from the central beam axis. However, the relative contribution of the forward directed unscattered protons increase at the proximal rise of the IDD curves as the ratios in Figure 4 converges towards unity. High energy protons are more likely to scatter in low angles when undergoing elastic scattering with the oxygen nucleus in the water phantom [1, 8, 26] and consequently a large fraction of the scattered protons will have a range rather close to that of the primary protons. The small discontinuity of the ratios observed before the Bragg peaks in Figure 4 is due to the Coulomb-nuclear interference effects described by Gerstein et al. [27]. This effect causes a local maximum of the proton differential cross section resulting in a higher yield of secondary protons for a specific angle and thus an increase in signal loss for the IC with limited diameter. The rather large signal losses showed that the low dose envelope originating from nuclear interactions of the primary protons expands over distances larger than the radius of the measurement IC and that this effect increases with incident proton energy. This emphasizes the need to quantify these signal losses and consequently correct the measured data when used as input for treatment planning systems.

The agreement between MCNP6 simulations and measurements supports the assumptions and input parameters employed in this work. The Monte Carlo model provided accurate representation of the beam characteristics with regard to absolute dose in water, range in water and lateral spot sizes in air. The ability to simulate accurate absolute dose IDD normalized to number of MU will prove useful for future studies regarding secondary dose assessment with MCNP6.

Acknowledgements
The authors would like to thank the physicists involved in the beam commissioning at the Skandion Clinic for providing depth dose curves, beam profile details and reference dosimetry data.

This work was partially supported by the Swedish Radiation Safety Authority under the contract SSM2016-2425. The authors declare no conflict of interest.

References

[1] Wilson R R 1946 *Radiology* **47** 487-91
[2] Paganetti H and Palmans H 2012 *Proton Therapy Physics*, ed H Paganetti (Boca Raton, Florida: CRC Press/Taylor & Francis) chapter 1, 7, 9
[3] Newhauser W D and Zhang R 2015 *Phys. Med. Biol.* **60** 155–209
[4] Paganetti H 2014 *Br. J. Radiol.* **87** 20140293
[5] Pedroni E, Scheib S, Böhringer T, Coray A, Grossmann M, Lin S and Lomax A *2005 Phys. Med. Biol.* **50** 541–61
[6] Li Y, Zhu R X, Sahoo N, Anand A and Zhang X 2012 *Phys. Med. Biol.* **57** 983–97
[7] Grevillot L, Bertrand D, Dessy F, Freud N and Sarrut D 2011 *Phys. Med. Biol.* **56** 5203–19
[8] Grassberger C, Lomax A and Paganetti H 2015 *Phys. Med. Biol.* **60** 633–45
[9] Schneider U, Agosteo S, Pedroni E and Besserer J 2002 *Int. J. Radiat. Oncol. Biol. Phys.* **53** 244–51
[10] Zacharatou Jarlskog C, Lee C, Bolch W E, Xu X G and Paganetti H 2008 *Phys. Med. Biol.* **53** 693–717
[11] Hultqvist M and Gudowska I 2010 *Phys. Med. Biol.* **55** 6633–53
[12] Goorley T et al. 2016 *Ann. Nucl. Energy.* **87** 772-83
[13] Taddei P J, Mirkovic D, Fontenot J D, Giebeler A, Zheng Y, Kornguth D, Mohan R and Newhauser W D 2009 *Phys. Med. Biol.* **54** 2259–75
[14] Titt U, Bednarz B and Paganetti H 2012 *Phys. Med. Biol.* **57** 6381–93
[15] Bielajew A F 2013 *Monte Carlo techniques in radiation therapy*, ed J Seco and F Verhagen (Boca Raton, FL: CRC Press/Taylor & Francis) chapter 1
[16] Randeniya S D, Taddei P J, Newhauser W D and Yepes P 2009 *Nucl. Technol.* **168** 810–14
[17] Newhauser W D, Rechner L, Mirkovic D, Yepes P, Koch N C, Titt U, Fontenot J D, and Zhang R 2013 *Radiat. Meas.* **58** 37–44
[18] Lee C C, Lee Y J, Tung C J, Cheng H W and Chao T C 2014 *Radiat. Phys. Chem.* **95** 302–4
[19] International Atomic Energy Agency 2006 *TRS 398-Absorbed Dose Determination in External Beam Radiotherapy: An International Code for Practice for Dosimetry based on Standards of Absorbed Dose to Water ver. 12* (Vienna: IAEA)
[20] *MCNP6 User's Manual Version 1.0* 2013 ed Pelowitz D B Los Alamos National Laboratory report LA-CP-13-00634
[21] Bertini H W 1963 *Phys. Rev.* **131** 1801–21
[22] Sawakuchi G O, Mirkovic D, Perles L A, Sahoo N, Zhu X R, Ciangaru G, Suzuki K, Gillin M T, Mohan R and Titt U 2010 *Med. Phys.* **37** 4960–70
[23] Anand A, Sahoo N, Zhu X R, Sawakuchi G O, Poenisch F, Amos R A, Ciangaru G, Titt U, Suzuki K, Mohan R and Gillin M T 2012 *Med. Phys.* **39** 891-900
[24] Clasie B, Depauw N, Fransen M, Gomà C, Panahandeh H R, Seco J, Flanz J B and Kooy H M 2012 *Phys. Med. Biol.* **57** 1147–58
[25] Gottschalk B, Cascio E W, Daartz J, Wagner M S 2015 *Phys. Med. Biol.* **60** 5627–54
[26] Braunn B, Boudard A, David J C, Koning A J, Leprince A, Leray S and Mancusi D 2015 *Eur. Phys. J. Plus* **130** 153
[27] Gerstein G, Niederer J and Strauch K 1957 *Phys. Rev.* **108** 427–32